# Nature of ground and electronic excited states of higher acenes

Yang Yang[a], Ernest R. Davidson[b,1], and Weitao Yang[a,c,d,1]

[a]Department of Chemistry, Duke University, Durham, NC 27708; [b]Department of Chemistry, University of Washington, Seattle, WA 98195; [c]Department of Physics, Duke University, Durham, NC 27708; and [d]Key Laboratory of Theoretical Chemistry of Environment, Ministry of Education, School of Chemistry and Environment, South China Normal University, Guangzhou 510006, China

Edited by Michael L. Klein, Temple University, Philadelphia, PA, and approved July 6, 2016 (received for review April 15, 2016)

**Higher acenes have drawn much attention as promising organic semiconductors with versatile electronic properties. However, the nature of their ground state and electronic excited states is still not fully clear. Their unusual chemical reactivity and instability are the main obstacles for experimental studies, and the potentially prominent diradical character, which might require a multireference description in such large systems, hinders theoretical investigations. Here, we provide a detailed answer with the particle–particle random-phase approximation calculation. The $^1A_g$ ground states of acenes up to decacene are on the closed-shell side of the diradical continuum, whereas the ground state of undecacene and dodecacene tilts more to the open-shell side with a growing polyradical character. The ground state of all acenes has covalent nature with respect to both short and long axes. The lowest triplet state $^3B_{2u}$ is always above the singlet ground state even though the energy gap could be vanishingly small in the polyacene limit. The bright singlet excited state $^1B_{2u}$ is a zwitterionic state to the short axis. The excited $^1A_g$ state gradually switches from a double-excitation state to another zwitterionic state to the short axis, but always keeps its covalent nature to the long axis. An energy crossing between the $^1B_{2u}$ and excited $^1A_g$ states happens between hexacene and heptacene. Further energetic consideration suggests that higher acenes are likely to undergo singlet fission with a low photovoltaic efficiency; however, the efficiency might be improved if a singlet fission into multiple triplets could be achieved.**

higher acenes | diradical | double excitation | particle–particle random-phase approximation | charge-transfer excitation

Organic semiconductors can potentially replace their conventional inorganic counterparts with less manufacturing cost and more flexibility over a large but light substrate. They have been widely used in organic light-emitting diodes (OLEDs), organic field-effect transistors (OFETs), and organic photovoltaic cells (OPVs). Some of the organic semiconductors are able to undergo singlet fission, a multiexciton generation process which may dramatically increase solar cell efficiency. Acenes (Fig. 1) and their derivatives are a typical organic semiconductor material that is being intensively studied (1–4). With the increase of the oligomer length, the acenes display a rapid evolution of electronic structure and molecular properties, which greatly attracts the scientific community. The smallest naphthalene (**2**) and anthracene (**3**) are stable species that can be isolated from coal or petroleum resources. They are widely used as basic synthetic blocks (5, 6). The larger tetracene (**4**) and pentacene (**5**) are promising organic semiconductors and have been applied as OFETs (7–17) thanks to a low vibrational reorganization energy and therefore a high hole mobility (18). Many of the derivatives of **4** and **5** are good candidates for OLEDs (19–22). Recently, with a growing interest in solar energy and solar cells, **4** and **5** have also been made into OPV devices (23–27). Furthermore, **3–5** have been shown to be able to undergo singlet fission (28–33) ($^1M^* + {}^1M \rightarrow 2\ {}^3M^*$), which in principle can raise the efficiency limit of a solar cell to more than 40% (34, 35) by converting one high-energy singlet exciton to two spatially separated lower-energy triplet excitons. Higher acenes with more than five linearly fused benzene rings are believed to possess more tempting electronic structure and molecular properties (3, 4, 36). However, the instability of the higher acenes remains a main obstacle to experimental research. Even though the synthesis of hexacene (**6**) was reported more than 70 y ago (37, 38), a scheme that is easy to reproduce was not achieved until 2007 through a photochemical process in a polymer matrix, which helps retain the highly reactive product **6** (39). Similar schemes were also successfully applied to the synthesis of three even less stable species—heptacene (**7**) (40), octacene (**8**), and nonacene (**9**) (41). Although the synthesis of decacene (**10**) and undecacene (**11**) with 10 or more fused-benzene rings will be more challenging and has not yet been achieved, the exploration of higher acenes and their derivatives continues unabated.

In contrast to these fruitful experimental studies, there are relatively fewer systematic theoretical studies on higher acenes.

The nature of the ground state of higher acenes still remains controversial. Is the ground state a triplet, a closed-shell singlet, or an open-shell singlet? How significant is the diradical character? What is the singlet–triplet (ST) gap limit for polyacene? The answer to these questions concerns the molecular properties of higher acenes, and it is an important challenge, particularly in the absence of accurate experimental characterization. Unfortunately, the large system size of higher acenes hinders the use of many accurate but expensive theoretical tools. Empirical or semiempirical studies (42–47) are inexpensive but also less accurate, and therefore seem to be less widely accepted. One of the most acknowledged theoretical predictions, up to now, is based on the unrestricted density-functional theory (UDFT) calculation performed more than 10 y ago (48). However, it is widely known that the utilization of broken-symmetry calculation is a limitation and

## Significance

**Higher acenes are promising organic semiconductors with versatile electronic properties. A better understanding of their ground- and electronic excited states will benefit further molecular design and future applications. However, their instability and multireference character have impeded experimental and theoretical studies. Here, we use the recently developed particle–particle random-phase approximation in combination with a diradical analysis to unveil the nature of their ground- and electronic excited states. The excitation energies are presented, along with a detailed description of the bonding nature, which switches from regular molecules to full diradicals, and then even to polyradicals. The likelihood of singlet fission is briefly discussed from an energetic perspective.**

Author contributions: E.R.D. and W.Y. designed research; Y.Y. performed research; Y.Y. and E.R.D. analyzed data; and Y.Y., E.R.D., and W.Y. wrote the paper.

The authors declare no conflict of interest.

This article is a PNAS Direct Submission.

[1]To whom correspondence may be addressed. Email: erdavid@earthlink.net or weitao.yang@duke.edu.

This article contains supporting information online at www.pnas.org/lookup/suppl/doi:10.1073/pnas.1606021113/-/DCSupplemental.

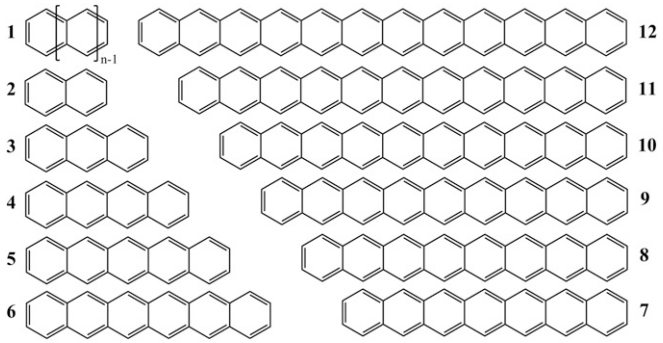


**Fig. 1.** Structure of acenes in one Kekule resonance form.

the breaking of spin symmetry is unphysical. Therefore, the broken-symmetry determinant of UDFT contains limited information of the entire many-electron wave function, and it may not describe the nature of the ground state. In the past 10 y, some accurate but relatively inexpensive theories have been developed and applied to higher acenes (49–57). Among them, the most widely accepted one seems to be the density matrix renormalization group method in combination with the complete active-space configuration interaction theory (49). It provided valuable insights into the ground state of higher acenes with a natural orbital analysis. Nonetheless, the computation is still demanding, and acenes longer than **6** were computed with the minimal basis set, which leads to uncertainty to the overall quantitative accuracy.

The ground state is already difficult to describe, let alone the more challenging excited states (58–63). As a result of a "charge separation in disguise" (61, 64), time-dependent density functional theory (TDDFT) is known to greatly underestimate the $^1B_{2u}$ excitation (65, 66), which is the lowest bright excitation for acenes longer than **2**, and is characterized by one electron promoted from the highest occupied molecular orbital to the lowest unoccupied molecular orbital (HOMO→LUMO). Moreover, because of a double-excitation nature, the description of the dark $^1A_g$ state is completely unattainable by the commonly used adiabatic TDDFT (67–71). Unfortunately, this dark state is particularly important to researchers as it has been proposed as a crucial intermediate in the process of singlet fission (33). Only some expensive multireference methods (32, 33, 72–74) have hitherto been applied to describe this $^1A_g$ state for small acenes, but these methods are not feasible for higher acenes because of the computational cost. Very recently, the DFT-based multireference configuration interaction method (DFT/MRCI) has been applied to the excited states of higher acenes up to **9** and achieved good accuracy (63). However, only the lowest few bright excited states were investigated and the bonding nature of those states was not fully elaborated.

In this work, we provide both qualitative and quantitative descriptions on the nature of the ground and electronic excited states of higher acenes. The quantitative calculation is based on the particle–particle random-phase approximation (pp-RPA). This method was recently introduced to quantum chemistry to calculate the correlation energy of a ground state in combination with both Hartree–Fock (HF) theory and DFT (75–80). It was later further extended to describing excitations (81–84). For excited states calculation, it starts from a two-electron deficient ($N-2$) system described with DFT correlation, then recovers a series of neutral states by adding back two explicitly correlated electrons. It describes the ground state and electronic excited states on the same footing. In practice, even though it intrinsically misses non-HOMO excitations, the pp-RPA has been demonstrated to be able to solve such greatly challenging problems as double excitations, Rydberg excitations, charge-transfer excitations, ST gaps for diradical systems, as well as regular HOMO-dominated single excitations (81, 83, 85, 86). According to the benchmark studies (83, 85), the Becke-3–Lee–Yang–Parr (B3LYP) functional generally provides an $N-2$ reference that gives rise to reliable pp-RPA excitation energies and has fewer convergence difficulties. In contrast, the HF functional often yields larger error whereas the Perdew–Burke–Ernzerhof functional frequently encounters $N-2$ convergence problems. Therefore, in this work, we use pp-RPA-B3LYP for quantitative analysis. Our qualitative analysis is based on the homosymmetric diradical discussion by Salem and Rowland (87). For a simple analogy, we use the simplest stretched $H_2$ diradical model, as in existing literature (88). Although these qualitative analysis techniques can be found in decades-old papers, we here present them to aid our analysis of higher acenes. At the end of the paper, the feasibility of undergoing singlet fission for higher acenes is briefly discussed purely from an energetic perspective.

## Results

**ST Energy Gap.** We here refer to the ST energy gap as the transition energy from the lowest $^1A_g$ to the lowest $^3B_{2u}$ state ($E_T$–$E_S$). We use optimized geometries for the neutral $N$-electron molecule obtained with the B3LYP function with the 6-31G* basis set (B3LYP/6-31G*). Three set of geometries are used, which are optimized by restricted singlet (R), unrestricted singlet (U), and unrestricted triplet (T), respectively. Table 1 shows the results from the pp-RPA calculation with the B3LYP functional and the double-ζ correlation consistent basis set (pp-RPA-B3LYP/cc-pVDZ). We predict the ground state of higher acenes to be singlet rather than triplet, and it is so even at the optimized geometry for the neutral triplet state (T geo). This agrees with many recent predictions (46, 48–52, 55, 89). With the increase of the acene size, the ST gap decreases. Compared with experimental data, our theoretical predictions consistently overestimate ST gaps by around 0.15 eV at geometries optimized by restricted singlet (R geo) while underestimating them at T geo. This is probably because the experimental data are possibly closer to adiabatic gaps whereas theoretical predictions are for vertical gaps at a fixed geometry. Therefore, these two prediction series at R and T geometries are expected to provide the upper and lower bounds for the adiabatic ST gaps. We fit the two series with the simple exponential decay formula ($E = ae^{-n/b} + c$) and plot the result in Fig. 2. The predicted gap limit is between 0.0 and 0.1 eV, which is still positive but vanishingly small. This small ST gap also indicates a probable diradical or polyradical nature for higher acenes, which

**Table 1. Excitation energy (in electron volts) of $^3B_{2u}$ state**

| Acene | 2 | 3 | 4 | 5 | 6 | 7 | 8 | 9 | 10 | 11 | 12 |
|---|---|---|---|---|---|---|---|---|---|---|---|
| pp-RPA@R | 2.87 | 1.98 | 1.39 | 0.98 | 0.70 | 0.51 | 0.37 | 0.28 | 0.22 | 0.18 | 0.16 |
| pp-RPA@U | 2.87 | 1.98 | 1.39 | 0.98 | 0.66 | 0.39 | 0.23 | 0.15 | 0.11 | 0.11 | 0.13 |
| pp-RPA@T | 1.99 | 1.35 | 0.90 | 0.59 | 0.39 | 0.25 | 0.17 | 0.12 | 0.09 | 0.09 | 0.11 |
| Experiment | 2.65* | 1.87† | 1.27‡ | 0.86§ | — | — | — | — | — | — | — |

—, Data not available from literature.
*Ref. 117.
†Ref. 118.
‡Ref. 119.
§Ref. 120.

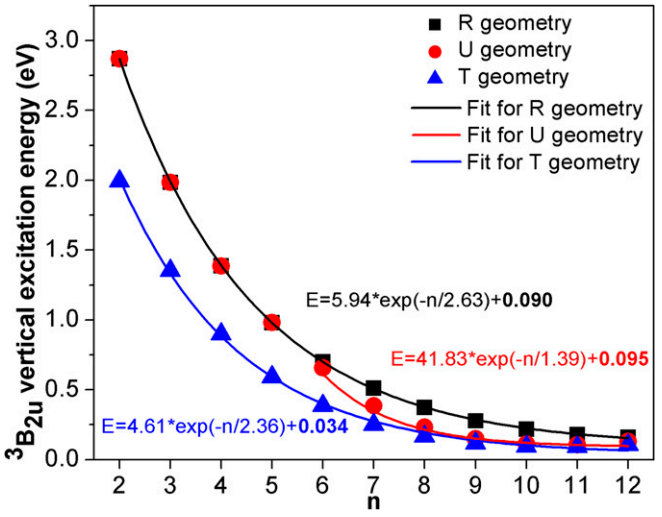


**Fig. 2.** Vertical triplet excitation energy from pp-RPA for acenes with restricted singlet geometry (R), unrestricted singlet geometry (U), and triplet geometry (T). The R and T series approximately provide upper and lower bounds for the adiabatic ST gaps. The U series first coincides with R and then differs from R starting from **6**. Because the U − R difference is an essential discontinuity for the U series, it is fitted starting from **6**. The constant term in the exponential fit provides the limit for polyacenes. The predicted ST gap in the limit is vanishingly small and is about 0.0–0.1 eV.

we will discuss more in *Singlet Ground State in the Diradical Continuum*.

The ST gaps at geometries optimized by unrestricted singlet (U geo) are also plotted. It can be seen that they first coincide with R results and later resemble T results. Therefore, their ST gap decreases much faster. Because there is an essential discontinuity between the shorter acenes where U converges to R and the longer ones where it gives different results, we perform the exponential extrapolation for acenes starting from **6**, whose U result begins to differ from R result. The gap limit is also vanishingly small between 0.0 and 0.1eV. It should be noted that if we adopt the whole U series for extrapolation, the gap limit is −0.02 eV. We expect it to be unphysically too low due to the discontinuity. This phenomenon is similar to the dissociation of $H_2$, in which there is a break in the slope at a critical bond length with unrestricted Hartree–Fock (UHF).

It is also worth noting that after removing the two outermost electrons, many diradical systems become closed-shell dications that can be well described by restricted DFT. The stable dication species can be perceived as a frozen core that makes a limited contribution to the dynamic correlations on both ground states and excited states. Acenes have been known to be such kind of molecules with stable dications (90). Because pp-RPA starts with a DFT calculation on this $N-2$ system, its overall accuracy benefits from the stability of acene dications.

**Singlet Ground State in the Diradical Continuum.** For a diradical system, besides the ST gap, the energy gap between the open-shell singlet and closed-shell singlet is also important. In the acene case, this question is the same as whether the ground state is open-shell or closed-shell because the ground state has already mostly been predicted to be singlet.

Chemists normally define open-shell and closed-shell with the help of molecular orbitals (MOs), because many chemical species can be approximately described by a single Slater determinant based on MOs. If two outermost electrons with opposite spins occupy the same MO, it is a closed-shell singlet; if they form a singlet but occupy different MOs, it is an open-shell singlet. Our study on acenes starts with this definition. Nonetheless, it should also be noted that this intuitive single-determinant picture collapses when a system has strong static correlation and therefore needs multireference for an accurate description. Many diradicals are such kind of systems. The multireference character, which may be reflected by the contribution from the dominant configuration in a configuration interaction (CI) manner, can work as an indicator of the diradical character. Using pp-RPA, which seamlessly combines DFT with the wave-function–based CI (85), we are able to analyze the diradical character of higher acenes.

The dominant configuration contribution (DCC) of a state, which we define as the square of the largest number in its corresponding pp-RPA matrix eigenvector, works as the indicator of the multireference character. The larger the DCC, the less the multireference character, and the more likely that this state can be well described with a single reference. The DCCs for acenes at different geometries are plotted in Fig. 3. For the first acene **2**, the single reference picture is completely valid because the dominant configuration with two electrons occupying HOMO contributes more than 99% to the ground state. The remaining contributions mainly come from the one with two electrons occupying LUMO rather than HOMO. With this 99% DCC, we assign the ground state of **2** to be an almost pure closed-shell singlet. As the acene fuses more benzene rings, the DCC gradually decreases. With the R geometries, it drops from 99% for **2**, to 95% for **8**, to 90% for **10**, and eventually to 75% for dodecane (**12**) at an accelerating speed. Nonetheless, all of them keep the $A_g$ symmetry. For the same acene, with a different geometry, the DCC for R is larger than that for T, and the result for U mostly lies in between, although it may finally cross over T for **11** and **12**. Among all of the cases, the smallest DCC happens to the U geometry for **12,** where it is only 42% and almost the same as the weight of the second dominant configuration, with the remaining 16% contribution coming from other configurations.

With a gradually decreasing DCC, the assignment of closed-shell and open-shell becomes tricky, so let us first consider the two-orbital diradical model (87). The extreme case is that the DCC is 50%, with the two electrons occupying HOMO having

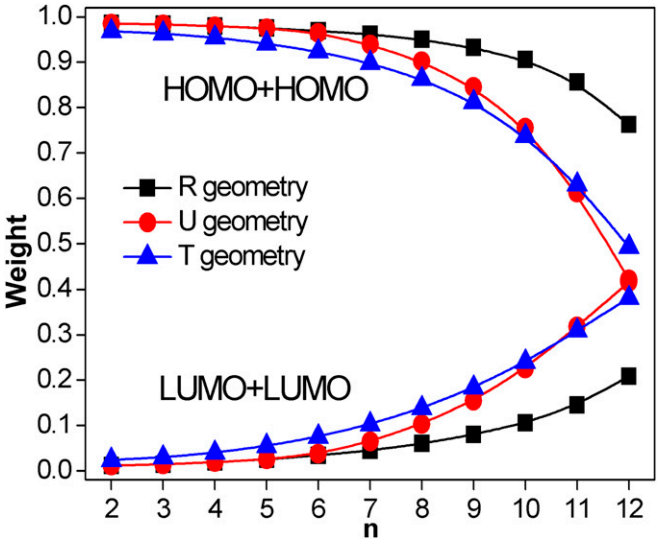


**Fig. 3.** First (two outermost electrons both added to HOMO) and second (two outermost electrons both added to LUMO) dominant configurations of the ground state for acenes with restricted singlet geometry (R), unrestricted singlet geometry (U), and triplet geometry (T). The contribution from the first DCC decreases with the increasing size of acenes, but up to **10** it is always larger than 0.75, which suggests that these acenes lie more on the closed-shell side. The DCC is higher with an R geometry than with a T geometry. The results from U geometry mostly lie in and shift from close to R to close to T, indicating a spin-symmetry broken solution. The U series finally crosses the T series and displays an almost full diradical character with similar contributions from the first and second DCCs. Meanwhile, the total contribution from the first two DCCs gradually decreases, suggesting the beginning of a polyradical nature.

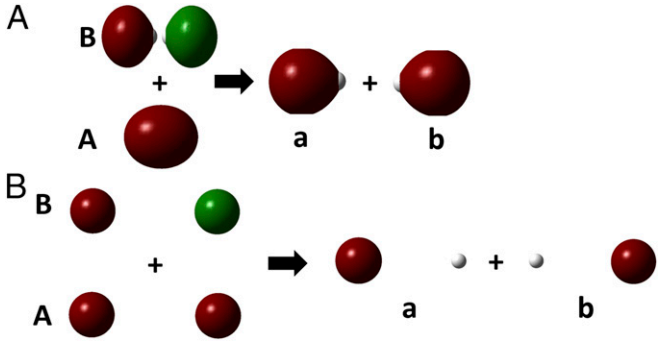


**Fig. 4.** Shape of delocalized frontier molecular orbitals (A and B) and localized transformed atomic-like orbitals (a and b) for $H_2$ at equilibrium geometry (*A*) and stretched geometry (*B*). Note the decreasing spatial overlap between a and b.

equal contribution to the configuration with the two electrons occupying LUMO. Note that the assignment of HOMO and LUMO is not so important in this case because they could in principle be degenerate. We simply call these two configurations "HOMO pair" and "LUMO pair," respectively. If we write the two MOs as A and B, the singlet ground state can be denoted as

$$\frac{1}{\sqrt{2}}\left(|A\bar{A}\rangle - |B\bar{B}\rangle\right), \qquad [1]$$

with opposite signs in front of the two configurations. Viewing from the valence bond perspective and performing the following unitary orbital transformation $a = 1/\sqrt{2}(A+B), b = 1/\sqrt{2}(A-B)$, we can rewrite Eq. **1** as

$$\frac{1}{\sqrt{2}}\left(|a\bar{b}\rangle - |\bar{a}b\rangle\right). \qquad [2]$$

The stretched $H_2$ at the stretched limit is the simplest case in this model and the shapes of its transformed orbitals *a* and *b* during the stretch process are plotted in Fig. 4 together with the original MOs *A* and *B*. It can been seen that *a* mostly localizes on one atom of the molecule while *b* localizes on the other, and the longer the bond stretches, the more localized these transformed orbitals are and the less overlap they have. Note that the shape of the transformed orbitals look like the singly occupied molecular orbitals (SOMOs) obtained from UDFT, which gives correct energy curve for $H_2$ stretched limit. For this extreme case, usually we no longer define "open-shell" or "closed-shell" in terms of the completely delocalized MOs *A* and *B*. Instead, we focus on the spatially localized atomic-like orbitals *a* and *b*. Because the two electrons separately occupy *a* and *b* and get spatially disconnected, it is open-shell. Therefore, most molecules ($|A\bar{A}\rangle$) with nearly 100% DCC are closed-shell and have "regular covalent" nature, whereas extreme diradicals ($1/\sqrt{2}(|A\bar{A}\rangle - |B\bar{B}\rangle)$) with 50% DCC are open-shell and have "diradical covalent" nature. (In valence bond theory, regular covalent has half ionic contribution whereas diradical covalent is purely covalent.) Those cases in between lie in the transitional region which in this paper we call the "diradical continuum." In the diradical continuum, it becomes meaningless to strictly label a species with open-shell or closed-shell, but here we can provide a qualitative distinction: if we set 75% DCC as the middle of the continuum, then those cases with more than 75% DCC are on the closed-shell side while those with less are on the open-shell side.

The case for acenes is highly similar, although slightly more complicated because more orbitals rather than only two may be involved. The HOMO and LUMO orbitals and their transformed orbitals are plotted in Fig. 5 for **6** (also see *SI Appendix*, Fig. S2 for **11** with odd number of benzene rings). There are also plots for HOMO-1 and LUMO+1 that will be discussed in *Doubly Excited* $^1A_g$ *State*. For the current ground-state discussion, we can simply focus on HOMO and LUMO because, as is shown above, the HOMO pair and LUMO pair configurations have largest weight up to **12**. The transformed orbitals for HOMO and LUMO localize on either edge of the acene molecules, and the more fused-benzene rings, the more separated they are. Note how similar they are to the SOMOs in the existing literature (48). We can roughly think of the ring-fusing process of acenes having the same effects as the stretching process of $H_2$, although the fusing is on the long axis whereas the orbital localization is with respect to the perpendicular short axis. If the ground state of an acene is completely dominated by the HOMO pair configuration, for example, **2** at R geometry, it is without doubt a closed-shell species; if nearly half contribution comes from the HOMO pair and the other half from the LUMO pair, for example, **12** at U geometry, then it is open-shell and almost a full diradical. The remaining cases in between are in the diradical continuum. The ground state of **10** at its U and T geometries and the ground state of **12** at R geometry have a DCC around 75%, and they roughly lie in the middle of the continuum. Because we already know the ground state is singlet rather than triplet, the R and U geometries should be closer to the true ground-state geometry than T geo. Between the R and U, because we find the ground states for acenes up to **10** have more closed-shell character, and the U calculation was more and more contaminated by the triplet state, we believe the R geo is more reliable for these acenes. For **11** and **12**, because more and more diradical and even polyradical character are added, we expect the true geometry is somewhere between U and R results, with a ground-state nature more and more to the open-shell.

Note that we use DCC based on a molecular orbital picture for the *N*−2 system to describe the diradical character. This is unique for pp-RPA. Because of the potential strong static correlation in

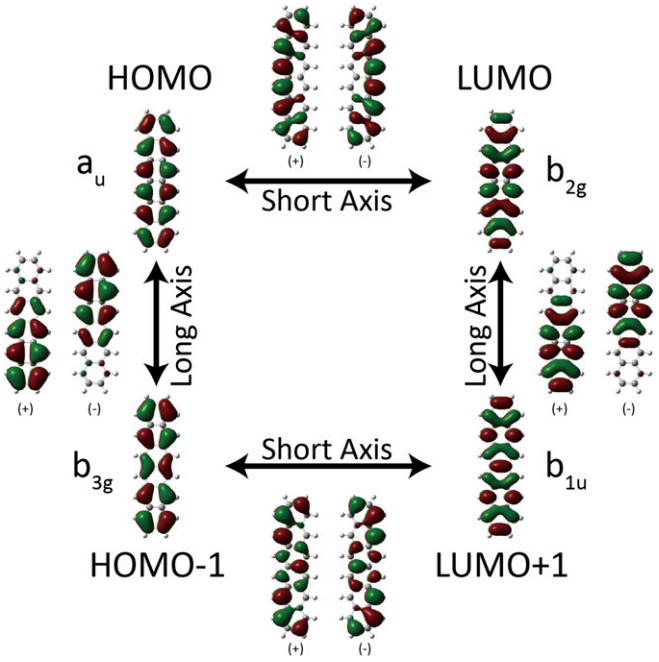


**Fig. 5.** Shape of delocalized MOs and transformed localized orbitals for **6**. All orbitals involved are π-orbitals. The HOMO is in fact LUMO for the *N*−2 reference, and it has $a_u$ symmetry. The LUMO (LUMO+1 for *N*−2) has $b_{2g}$ symmetry. Adding or subtracting HOMO and LUMO makes two localized orbitals along the short axis. The HOMO−1 (HOMO for *N*−2) has $b_{3g}$ symmetry and LUMO+1 (LUMO+2 for *N*−2) has $b_{1u}$ symmetry and adding or subtracting them also makes two localized orbitals along the short axis. The HOMO and HOMO−1 can make localized orbital pairs along the long axis and same for LUMO and LUMO+1.

neutral diradical systems, previously the natural orbital occupation analysis in combination with complete active space theory (49) or projected HF (53) has been used. These are wave-function–based methods and provide useful information of the ground-state wave function. However, the natural orbital analysis is less intuitive than MO analysis, and moreover it is considered to assign too much diradical character to the closed-shell **2** (49, 50). In contrast, the molecular orbital based on Kohn–Sham DFT is more intuitive and has been argued to be very suitable for qualitative chemical applications (91–93). Although, strictly speaking, the transitional amplitude of pp-RPA only describes the pairing density response to a pairing field (82), it can also be perceived that pp-RPA combines seamlessly a DFT description of the $N-2$ core electrons and a CI wave-function description of the outermost two electrons. It is thus possible to use molecular orbitals to reveal the nature of an excitation. This is similar in spirit to the well-known TDDFT, whose transitional amplitude only describes a density response to an external potential but is also used to explain the nature of an excitation based on a Kohn–Sham MO (94). Furthermore, unlike the natural orbital analysis, the nearly closed-shell description of **2** by pp-RPA agrees well with the generally accepted consensus. Therefore, the DCC descriptor based on the MO picture of the two-electron deficient system should be reliable in describing the diradical character.

What will the ground state be for even higher acenes beyond **12**? First, although in this work the optimized geometries for acenes up to **12** all collapse to the $D_{2h}$ point group, it does not necessarily mean that it will always keep such a high symmetry without any Jahn–Teller distortion or Peierls distortion as the number of benzene rings becomes even larger. In fact, some existing literature has already pointed out the possibility (95). Second, even if we assume the absence of the distortion and trust a geometry with $D_{2h}$ symmetry, from Fig. 3, we can see that the DCC later decreases very rapidly even at the R geometry, and meanwhile the total weight of the first two dominant configurations (HOMO pair and LUMO pair) decreases while the weight of the LUMO+1 pair increases. Usually the emergence of the LUMO+1 pair correlates with the breaking of the HOMO−1 pair, which is therefore an indirect sign for a polyradical character. Although for **11** and **12** we conclude the ground state might be more on the open-shell side of the diradical continuum, we also find that for **12**, the contribution from configurations other than the first two dominant ones has already been above 15% with the U geometry, suggesting an emerging polyradical character. Note that this polyradical nature was also observed by natural orbital analysis (49, 53, 54), and was claimed to emerge as early as **8** (54), but based on our analysis it does not show up until **11** and **12**. We anticipate the ground state of even higher acenes will possess even more polyradical character. With more and more polyradical character, it also becomes more and more challenging for current pp-RPA, because the pp-RPA assumes the electron pair occupying HOMO−1 will not break and therefore only explicitly correlates the two outermost electrons. In these cases, a multiconfiguration method that is able to excite even lower electrons is required.

Before we finish up our discussion on the ground state of higher acenes, we want to discuss UDFT calculations, which currently seem to be widely accepted. If we calculate using UHF or UDFT for both $H_2$ and acenes, at some point in the diradical continuum we will observe the energy deviation from the restricted theory. The orbitals obtained become two SOMOs and their shape resembles the transformed orbitals (45, 48). Although the energy from UHF or UDFT is usually more accurate than RHF or RDFT, the broken-spin-symmetry solution of UHF or UDFT does not lead to a correct wave-function description nor to a conclusion that the ground state has already become an open-shell singlet. According to the basic quantum mechanics, the spin symmetry broken under a spin-symmetric Hamiltonian is unphysical and there should not be any localized net spins without any perturbative observations. This deviation between unrestricted and restricted calculations simply raises a concern for those methods based on a single reference without considering static correlation. In this case, to achieve both accurate energy and meaningful wave function that describes the degree of the diradical character, one should refer to methods with a reference state maintaining proper spin symmetry, which usually means a multireference-based method, rather than literally interpreting the UDFT determinants. This statement should also apply to many current research projects concerning graphene fragments and spins on graphene edges.

**Lowest Bright Singlet Excitation.** We next look into the vertical excitations. For acenes longer than **2**, the singlet HOMO→LUMO excitation is the lowest bright singlet excitation. Considering the symmetry of the orbitals involved, this excitation can be denoted as $^1B_{2u}$. In addition, it is also widely known as the "p band" or "$L_a$ excitation" (1, 96). The excitation energies for this state are listed in Table 2 and plotted in Fig. 6. With the increasing number of benzene rings, as expected, there is a decreasing trend for the excitation energy. Note that because acenes up to **10** are more on the closed-shell side, the results at R geometry should be more reliable, and those with U and T geometry may underestimate the excitation. For **11** and **12**, the values at all three geometries are fairly close. There have been many studies on this excitation for acenes up to **6**, both experimentally and theoretically (33, 39, 58–66, 72–74, 97–104). For these acenes, except for **2**, in which the pp-RPA overestimates the excitation energy by 0.3 eV, our predictions match well with experiments, and the deviation is mostly within 0.05 eV. This small

**Table 2. Excitation energy (in electron volts) of $^1B_{2u}$ state**

| Acene | 2 | 3 | 4 | 5 | 6 | 7 | 8 | 9 | 10 | 11 | 12 |
|---|---|---|---|---|---|---|---|---|---|---|---|
| pp-RPA@R | 4.97 | 3.65 | 2.82 | 2.26 | 1.86 | 1.58 | 1.36 | 1.20 | 1.08 | 0.99 | 0.93 |
| pp-RPA@U | 4.97 | 3.65 | 2.82 | 2.26 | 1.83 | 1.49 | 1.26 | 1.12 | 1.02 | 0.96 | 0.94 |
| pp-RPA@T | 4.30 | 3.18 | 2.46 | 1.98 | 1.64 | 1.40 | 1.23 | 1.11 | 1.02 | 0.96 | 0.93 |
| CC2* | 4.88 | 3.69 | 2.90 | 2.35 | 1.95 | — | 1.43 | — | — | — | — |
| DFT-MRCI | 4.66[†] | 3.51[†] | 2.74[†] | 2.22[†], 2.16[‡] | 1.85[†], 1.80[‡] | 1.57[‡] | 1.44[†], 1.43[‡] | 1.34[‡] | — | — | — |
| Experiment | 4.66[§] | 3.60[§] | 2.88[§] | 2.37[§], 2.3[¶], 2.21[#], 2.22[‖] | 1.89[#], 1.80**, 1.85[††] | 1.50[‡‡], 1.70[#] | 1.54[§§] | 1.43[§§] | — | — | — |

—, Data not available from literature.
*CC2/cc-pVTZ result from ref. 65.
[†]Ref. 73.
[‡]Ref. 63.
[§]Refs. 65, 99.
[¶]Ref. 104.
[#]Ref. 101.
[‖]Ref. 102.
**Ref. 103.
[††]Ref. 39.
[‡‡]Ref. 40.
[§§]Ref. 41.

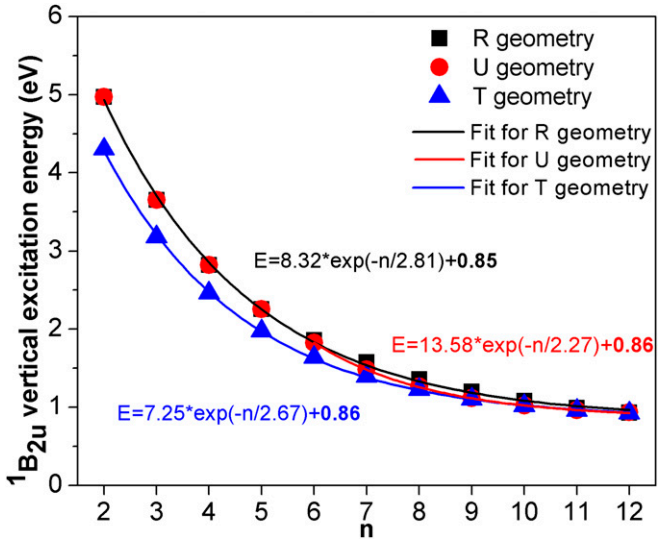


**Fig. 6.** Vertical excitation energy of $^1B_{2u}$ state for acenes with restricted singlet geometry (R), unrestricted singlet geometry (U), and triplet geometry (T). Because the ground states up to **10** are all closer to the closed-shell side, the R series provides a more reliable prediction, whereas for **11** and **12**, all geometries give similar results. The T series provides smaller numbers than the R series. The U series first coincides with R and later approaches T. Based on exponential decay fitting, the predicted polyacene limit of this vertical excitation is around 0.85 eV.

error is in sharp contrast with TDDFT, which underestimates the excitation energy by 0.4–0.5 eV with the same B3LYP functional (65). For higher acenes, we predict the excitation energy to be 1.58, 1.36, 1.20, 1.08, 0.96–0.99, and 0.93–0.94 eV for **7**, **8**, **9**, **10**, **11**, and **12**, respectively. We notice that some experimental data have been available for **7**, **8**, and **9** in polymer matrix or inert gas matrix (40, 41, 101), and there has been a fairly accurate DFT/MRCI study (63). It seems that our predictions might be slightly too low ($\approx$ 0.2 eV) for these higher acenes. However, now we are not sure of the reason, because both experimental and theoretical studies are at a rather preliminary stage. Relying on our current data, we perform the exponential fitting and predict the excitation energy for this state at the polyacene limit is around 0.85 eV.

The nature of the $^1B_{2u}$ state is less controversial than the ground state. This excitation is dominated by one electron excited from HOMO to LUMO, together with a small contribution from higher single excitation and even double excitations that can be neglected for acenes up to **12**. The dominant nature of this state can be denoted as

$$\frac{1}{\sqrt{2}}\left(|A\bar{B}\rangle - |\bar{A}B\rangle\right) = \frac{1}{\sqrt{2}}\left(|a\bar{a}\rangle - |b\bar{b}\rangle\right). \quad [3]$$

Salem and Rowland (87) call this state a zwitterionic state. Because the transformed orbitals *a* and *b* localize on the two opposite edges, there is a "hidden charge separation"—if we look at only one particular configuration, there is charge transfer, but if we look at the two together, there is no net charge transfer, nor any spin separation. It is worth noting that this orbital rotation trick to unveil the hidden charge separation has been used to explain the failure of TDDFT in describing this state (61). Because we previously made an analogy to the $H_2$ stretch process, here we just make one more comment on this resemblance. This excitation is similar to the ionic state reached as a result of "charge transfer" or "charge separation" excitation in stretched $H_2$. For stretched $H_2$, DFT and TDDFT fail to describe the ground state and this excited state (105–107) whereas the pp-RPA is exact with a special reference named HF* (81). Therefore, it is no wonder that pp-RPA is also able to describe this $^1B_{2u}$ state for acenes.

**Doubly Excited $^1A_g$ State.** To describe the double excitations in acenes is an even more challenging problem. To measure the excitation energies, experimentalists usually need to conduct nonlinear optics experiments with a two-photon process involved. For theoreticians, we can no longer perform the inexpensive adiabatic TDDFT calculation because it cannot capture double excitations (67–71). Fortunately, along with some expensive methods, the pp-RPA can handle well those double excitations excited from HOMO (81). The excitation energies for the lowest doubly excited state ($^1A_g$) are listed in Table 3 and plotted in Fig. 7. The molecule **5** is the one that has been studied most. Among those existing studies, considering the level of theory as well the basis set, the complete active space second-order perturbation theory on top of a state-averaged 14-electron and 14-orbital active space calculation with the triple-ζ ANO-L basis set [CASPT2/SA-CASSCF(14,14)/ANO-L-VTZP] should be the most accurate (72). Our prediction (2.74 eV) agrees well with its value (2.88 eV), whereas DFT-MRCI (58, 73) (2.52 eV) might systematically underestimate this whole $^1A_g$ series. The energy of this excitation also decreases with the size of the acene; however, it decreases much faster than the $^1B_{2u}$ excitation. In **2** and **3**, $^1A_g$ is over 1 eV higher than $^1B_{2u}$, whereas it becomes 0.4 eV lower in **10** and 0.6 eV lower in **12**. From our calculation, the order switch occurs between **6** and **7**, which is in accordance with a previous DFT-MRCI study (73). For **5**, the doubly excited state $^1A_g$ is about 0.5 eV higher than the singly excited $^1B_{2u}$; therefore, it is not quite likely that this doubly excited state would be involved in its singlet fission process (33). However, we do not refute the hypothesis that this $^1A_g$ state might play a role in the singlet fission process for acenes longer than **6**, in which it has become the lowest excited singlet state.

To the best of our knowledge, the nature of the $^1A_g$ state has not been discussed in detail due to the relatively scant studies. Here we will continue using the two-orbital diradical model for discussion.

For a species with barely any diradical character, such as $H_2$ near its equilibrium geometry, the ground state is $|A\bar{A}\rangle$, whereas

**Table 3. Excitation energy (in electron volts) of doubly excited $^1A_g$ state**

| Acene | 2 | 3 | 4 | 5 | 6 | 7 | 8 | 9 | 10 | 11 | 12 |
|---|---|---|---|---|---|---|---|---|---|---|---|
| pp-RPA@R | 6.43 | 4.87 | 3.65 | 2.74 | 2.05 | 1.54 | 1.14 | 0.84 | 0.61 | 0.43 | 0.31 |
| pp-RPA@U | 6.43 | 4.87 | 3.65 | 2.74 | 1.99 | 1.36 | 0.95 | 0.67 | 0.48 | 0.36 | 0.30 |
| pp-RPA@T | 5.31 | 3.94 | 2.92 | 2.17 | 1.61 | 1.20 | 0.89 | 0.67 | 0.51 | 0.40 | 0.33 |
| DFT-MRCI* | 5.73 | 4.60 | 3.37 | 2.52 | 1.86 | — | — | — | — | — | — |
| Other | — | — | — | 1.95†, 2.63‡, 2.88§ | — | — | — | — | — | — | — |

—, Data not available from literature.
*Refs. 58, 73.
†CASPT2(12,12)/cc-pVTZ result from ref. 33.
‡CASSCF(12π,12e) result from ref. 74.
§CASPT2/SA-CASSCF (14, 14)/ANO-L-VTZP result from ref. 72.

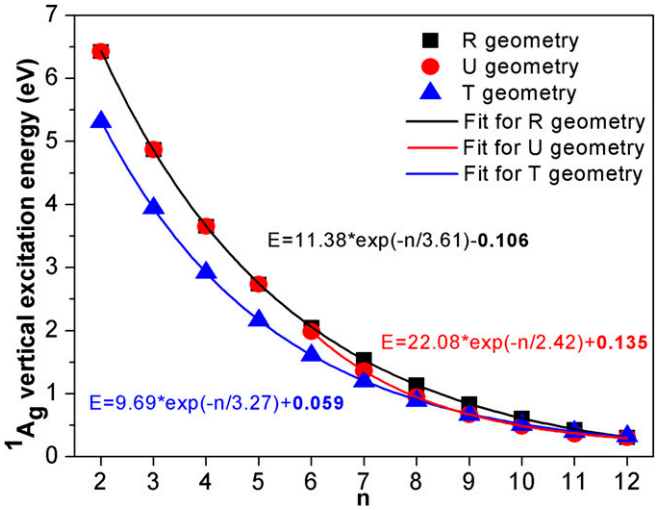


**Fig. 7.** Vertical excitation energy of $^1A_g$ excited state for acenes with restricted singlet geometry (R), unrestricted singlet geometry (U), and triplet geometry (T). Because the ground states up to **10** are all closer to the closed-shell side, the R series provides a more reliable prediction, whereas for **11** and **12**, all geometries give similar results. The T series provides smaller numbers than the R series. The U series first coincides with R, later approaches T, and finally even crosses below T. Based on exponential decay fit, the predicted polyacene limit of this vertical excitation can be vanishingly small. However, considering its zwitterionic nature with respect to the short axis, it should never become the ground state, and the negative limit by R series is an artifact introduced by extrapolation.

the doubly excited state is $|B\bar{B}\rangle$, both of which have "regular covalent" nature.

For a species in the diradical limit, such as the infinitely stretched $H_2$, as discussed earlier, the ground state is open-shell with a diradical covalent nature. In contrast, the doubly excited $^1A_g$ state in the diradical limit is

$$\frac{1}{\sqrt{2}}\left(|A\bar{A}\rangle + |B\bar{B}\rangle\right) = \frac{1}{\sqrt{2}}\left(|a\bar{a}\rangle + |b\bar{b}\rangle\right). \quad [4]$$

In the picture of MO theory, it differs from the ground state by only an opposite sign. Nonetheless, after the orbital transformation and then using the language of valence bond theory, this state becomes another zwitterionic state with hidden charge separation. Thus, it can also be seen as a closed-shell species, and this is in sharp contrast to the open-shell nature of the ground state.

It is also worth noting that in the diradical limit of the two-orbital model, with no overlap between the transformed orbitals $a$ and $b$, the two zwitterionic states $1/\sqrt{2}(|a\bar{a}\rangle - |b\bar{b}\rangle)$ and $1/\sqrt{2}(|a\bar{a}\rangle + |b\bar{b}\rangle)$ are degenerate. This happens with the stretched $H_2$, which is dominated by two orbitals.

For those species lying in the diradical continuum, the nature of their excited $^1A_g$ state lies in between above two extremes, and gradually shifts from a regular molecular species with more double-excitation nature to a diradical species with more zwitterionic nature.

The situation for acenes becomes much more complicated than this model. First, for small acenes, the $^1A_g$ state is not a pure doubly excited state; it has high excitation energy and combines with some high single-excitation configurations. It is similar to polyenes, whose $^1A_g$ state is a mixture of HOMO,HOMO→LUMO,LUMO, HOMO−1→LUMO, and HOMO→LUMO+1 (108, 109). However, because of the additional symmetry involved along the short axis of polyacenes, the next singly excited configuration that has the $^1A_g$ symmetry does not show up until fairly late compared with polyenes (mostly HOMO→LUMO+4 and also possibly HOMO−4→LUMO in the B3LYP orbital lineup for the neutral polyacene systems). Note here, because of the lack of non-HOMO excitations and therefore not being able to count in the HOMO−4→LUMO contribution for pp-RPA, our theoretical predictions on this state for those small acenes might be slightly overestimated. However, for these small acenes, these problems can be solved with higher accuracy wave-function methods, and here we mainly focus on higher acenes.

The contributions to this $^1A_g$ state from different configurations are plotted in Fig. 8. Starting from **5**, this state can be roughly seen as a double-excitation state, with the weight of the dominant configuration (LUMO pair) being around 75%, while the weight of its counterpart (HOMO pair) is only about 1%. If we now simply focus on these two configurations and consider the two-level diradical model, the higher acenes truly resemble the stretched $H_2$. With more and more fused-benzene rings, there is less and less contribution from the LUMO pair configuration, and more and more contribution from the HOMO pair configuration, which indicates a transition from the doubly excited $|B\bar{B}\rangle$ state to the zwitterionic $1/\sqrt{2}(|a\bar{a}\rangle + |b\bar{b}\rangle)$ state. However, this only reveals part of its nature. Unlike the ground state, in which the HOMO pair and LUMO pair configurations contribute more than 90%, the total weight of these two configurations is only around 50–70% for this state. Another part of the contribution comes from the LUMO+1 pair, which stands for a doubly excited configuration from HOMO to LUMO+1. As the weight of the LUMO pair decreases, the weight of the LUMO+1 pair also increases, just like the HOMO pair. Chemistry intuition tells us this correlation probably roots in an intrinsic orbital relation between LUMO and LUMO+1. We therefore plot LUMO+1 and its transformed orbital with LUMO (Fig. 5 and *SI Appendix*, Fig. S2). Interestingly, it can be clearly seen that these two orbitals can localize along the long axis under the orbital rotation. This means that if we completely ignore previous discussions on the HOMO pair and only focus on the current LUMO pair and LUMO+1 pair, we can obtain another two-level diradical model. The difference is that the

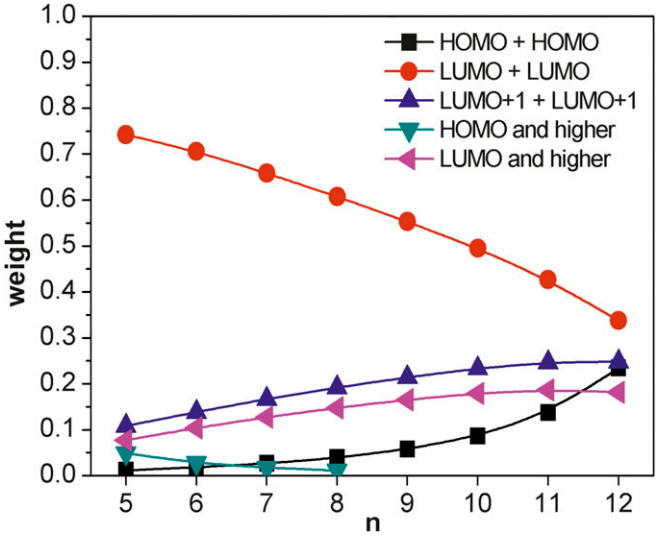


**Fig. 8.** Contributions from first few dominant configurations of the excited $^1A_g$ state for acenes (**5** to **12**) with restricted singlet (R) geometry. The contribution from the first DCC (LUMO pair) decreases with the increasing size of acenes. The increasing weight of HOMO pair indicates a diradical nature along the short axis, whereas the increasing weight of LUMO+1 pair indicates a diradical nature with respect to the long axis. The bonding nature of these two diradicals in the limit are zwitterionic and covalent, respectively. The decreasing weight for "HOMO and higher" suggests a decreasing contribution from a regular single excitation, which is important for shorter acenes (**2** to **4**). The increasing weight for "LUMO and higher" stands for an increasing weight for higher doubly excited configurations that is beyond the two orbital diradical models.

previous model concerns the short axis whereas this one is related to the long axis. We now denote the LUMO+1 as $C$ and its transformed orbital with LUMO as $b'$ and $c$. (Note this $b'$ is different from $b$.) In both of the diradical limits, these two "orthogonal" diradical pictures should be able to combine, and they can generate four $^1A_g$ states,

$$\frac{c_1}{\sqrt{2}}\left(|A\bar{A}\rangle - |B\bar{B}\rangle\right) + \frac{c_2}{\sqrt{2}}\left(|B\bar{B}\rangle - |C\bar{C}\rangle\right), \quad [5a]$$

$$\frac{c_1}{\sqrt{2}}\left(|A\bar{A}\rangle + |B\bar{B}\rangle\right) + \frac{c_2}{\sqrt{2}}\left(|B\bar{B}\rangle - |C\bar{C}\rangle\right), \quad [5b]$$

$$\frac{c_1}{\sqrt{2}}\left(|A\bar{A}\rangle - |B\bar{B}\rangle\right) + \frac{c_2}{\sqrt{2}}\left(|B\bar{B}\rangle + |C\bar{C}\rangle\right), \quad [5c]$$

$$\frac{c_1}{\sqrt{2}}\left(|A\bar{A}\rangle + |B\bar{B}\rangle\right) + \frac{c_2}{\sqrt{2}}\left(|B\bar{B}\rangle + |C\bar{C}\rangle\right), \quad [5d]$$

where $c_1$ and $c_2$ are combination coefficients and vary in each state. These states can be rewritten in terms of transformed orbitals

$$\frac{c_1}{\sqrt{2}}\left(|a\bar{b}\rangle - |\bar{a}b\rangle\right) + \frac{c_2}{\sqrt{2}}\left(|b'\bar{c}\rangle - |\overline{b'}c\rangle\right), \quad [6a]$$

$$\frac{c_1}{\sqrt{2}}\left(|a\bar{a}\rangle + |b\bar{b}\rangle\right) + \frac{c_2}{\sqrt{2}}\left(|b'\bar{c}\rangle - |\overline{b'}c\rangle\right), \quad [6b]$$

$$\frac{c_1}{\sqrt{2}}\left(|a\bar{b}\rangle - |\bar{a}b\rangle\right) + \frac{c_2}{\sqrt{2}}\left(|b'\overline{b'}\rangle + |c\bar{c}\rangle\right), \quad [6c]$$

$$\frac{c_1}{\sqrt{2}}\left(|a\bar{a}\rangle + |b\bar{b}\rangle\right) + \frac{c_2}{\sqrt{2}}\left(|b'\overline{b'}\rangle + |c\bar{c}\rangle\right). \quad [6d]$$

Therefore, the first state has diradical covalent nature along both short and long axes, the second state has zwitterionic nature along the short axis and diradical covalent nature along the long axis, the third state is completely opposite to the second one, and the fourth state has zwitterionic nature on both axes.

Further examination of the sign of the ground state and the lowest excited $^1A_g$ state of acenes suggests that the ground state is the same as the first state in nature and the excited $^1A_g$ state is the same as the second state. This energy alignment is easily understandable. First, with the help of a simple Hückel model (which we will not show in detail here), we know that the ionic state is higher in energy than its corresponding covalent state. Therefore, the doubly covalent state should be the lowest in energy, and the doubly ionic state should be the highest in energy. Second, intuitively speaking, the zwitterion along the short axis has less hidden charge separation character than that along the long axis, and thus should have lower energy. In this sense, even though some of our quantitative extrapolation (R series in Fig. 7) based on existing data suggests that the excited $^1A_g$ state might become the ground state with a negative limit, in principle it should never happen based on the qualitative analysis. This raises a warning for the results obtained from extrapolation, especially in the close-to-zero region, where a qualitative error might occur due to a quantitative uncertainty.

Despite the above lengthy discussion, the nature of this $^1A_g$ state is still far from being fully elaborated. Another orbital, which is the HOMO−1, can also play a role in this state. We previously only investigated the HOMO pair configuration and doubly excited LUMO pair (HOMO, HOMO→LUMO, LUMO) and LUMO+1 pair (HOMO, HOMO→LUMO+1, LUMO+1) configurations, but in fact, a fourth configuration, the doubly excited (HOMO−1, HOMO−1→LUMO,LUMO) may also be important. Unfortunately, because of the restrictions of the pp-RPA, which now is unable to describe non-HOMO excitations, we cannot provide detailed data. Nevertheless, we here provide some qualitative analysis. The (HOMO−1, HOMO−1→LUMO, LUMO) configuration is another counterpart to (HOMO, HOMO→LUMO, LUMO) configuration. The transformed orbitals concern HOMO and HOMO−1, and they localize along the long axis (Fig. 5 and *SI Appendix*, Fig. S2). It is also without doubt that there are many more configurations that can play a role, for example (HOMO−1, HOMO−1→LUMO+1, LUMO+1) is a counterpart of the Aufbau configuration and it correlates HOMO−1 and LUMO+1 along the short axis, but as a result of the large orbital energy difference, their contribution should be significantly smaller.

**Singlet Fission for Higher Acenes.** How likely are the higher acenes to be good candidates for singlet fission that can be used in photovoltaics? Three thermodynamic criteria are often used in an analysis (29, 110). The first criterion is $E(S_1) > 2E(T_1)$. When it is satisfied, the singlet-fission process is exoergic and hence is energetically favorable, whereas the reverting annihilation process is unfavorable. This is a desirable criterion for designing new molecules for singlet fission, although it may not be strictly satisfied because many organic molecules that are known to undergo singlet fission do not need to satisfy this thanks to possible thermal or artificial activations. According to our calculation, **4** is the smallest acene that satisfies the $E(S_1) > 2E(T_1)$ condition. This also agrees with experiments that the singlet fission observed in **4** and **5** does not need much energy activation (29, 111). The second condition is $E(T_2) > 2E(T_1)$. It simply keeps the two triplet states from annihilating and forming the second lowest triplet state. This condition is also easy to satisfy for acenes. From our calculation, we observe that it is always satisfied starting from **4**. (See *SI Appendix* for detailed data for $T_2$.) The third criterion is $E(S_1) \approx 2$ eV and $E(T_1) \approx 1$ eV. Strictly speaking, this is not a criterion for singlet fission, but a condition that favors high photovoltaic efficiency for practical applications. We find **5** to be the best molecule that satisfies this condition. For higher acenes that are longer than **5**, even though singlet fission is more energetically favorable, both the singlet and triplet excitations are much too low in energy and hence not good for high photovoltaic efficiency. However, even though not yet observed, the singlet fission does not necessarily only generate two triplets and these higher acenes might be good candidates for generating multiple triplets, which could benefit the efficiency if achievable (29). Purely from the energy perspective, **7** and **8** favor a singlet fission into three triplets, whereas **9** and **10** are potential to generate four. Therefore, after taking into account all three of these criteria, we anticipate that higher acenes are very likely to undergo singlet fission, but the energy conversion efficiency might be low because of a large system size and low excitation energies. If a singlet fission into multiple triplets can be achieved, then higher acenes might be promising materials for photovoltaic applications. However, it should be noted that because of the increasing diradical character and the high instability of higher acenes, before converting them into devices, one of the most urgent tasks now might be to find a condition to stabilize these species. This points out the importance of looking for more stable derivatives (3).

## Conclusion

In summary, we qualitatively and quantitatively described the nature of the ground- and lowest few important excited states of higher acenes. With the increasing number of fused-benzene rings, their ground state slides in the diradical continuum with more and more open-shell character. For acenes up to **10**, the ground state is on the closed-shell side, whereas for **11** and **12**, the ground state tilts more to the open-shell side. The polyradical character also emerges after **10**. The ground state always has $^1A_g$ symmetry and it has covalent nature with respect to both the short and long axes. The ST gap is predicted to be always positive but can be vanishingly small for the polyacene limit based on an exponential decay fitting. The $^1B_{2u}$ singlet excited state is a zwitterionic state with respect to the short axis, and its energy decreases slowly with the

acene size. The excited $^1A_g$ state also has a decreasing trend in excitation energy but it decreases faster than that of $^1B_{2u}$, rendering it the lowest singlet excited state starting from **7**. The nature of this $^1A_g$ state gradually switches from a regular doubly excited state to another zwitterionic state on the short axis with the increasing size of acenes, but always keeps its covalent nature with respect to the long axis. It in principle cannot become the ground state because the ground state should be covalent for both axes. Further consideration of the relative energies of $^1B_{2u}$ and the lowest two triplet excitations implies that higher acenes are likely to undergo singlet fission but with a relatively low photovoltaic efficiency. The efficiency might be improved if a singlet fission into multiple triplets can finally be achieved.

## Computational Details

The geometry optimization was conducted at the B3LYP/6–31G* level with the Gaussian09 program (112). No special restriction on the symmetry was applied, but finally all of them collapse to the $D_{2h}$ point group. The set of geometries is essentially the same as those in refs. 48, 49). with the same Kohn–Sham total energy for the molecules in common, but it is a more complete set which includes geometries from **2** to **12** optimized for R, U, and T states. The geometries can be found in *SI Appendix*, along with Kohn–Sham total energies and spin expectation values. A frequency check suggests that there is no imaginary vibrational mode. All pp-RPA calculation were carried out with the QM4D program (113). The B3LYP (114, 115) density functional and Dunning's correlation-consistent basis set (cc-pVDZ) (116) were adopted in the pp-RPA calculation.

**ACKNOWLEDGMENTS.** We thank Dr. Christopher Sutton and Mr. Du Zhang for helpful discussions. Y.Y. appreciates the support as part of the Center for the Computational Design of Functional Layered Materials, an Energy Frontier Research Center funded by the US Department of Energy, Office of Science, Basic Energy Sciences under Award DE-SC0012575. W.Y. appreciates the support from National Science Foundation (CHE-1362927).

1. Clar E (1964) *Polycyclic Hydrocarbons* (Academic, London), p v.
2. Bendikov M, Wudl F, Perepichka DF (2004) Tetrathiafulvalenes, oligoacenenes, and their buckminsterfullerene derivatives: The brick and mortar of organic electronics. *Chem Rev* 104(11):4891–4946.
3. Anthony JE (2006) Functionalized acenes and heteroacenes for organic electronics. *Chem Rev* 106(12):5028–5048.
4. Anthony JE (2008) The larger acenes: Versatile organic semiconductors. *Angew Chem Int Ed Engl* 47(3):452–483.
5. Collin G, Höke H, Greim H (2000) Naphthalene and hydronaphthalenes. *Ullmann's Encyclopedia of Industrial Chemistry* (Wiley-VCH, Weinheim, Germany), Vol 23, pp 661–670.
6. Collin G, Höke H, Talbiersky J (2000) Anthracene. *Ullmann's Encyclopedia of Industrial Chemistry* (Wiley-VCH, Weinheim, Germany), Vol 2, pp 497–501.
7. Takeya J, et al. (2003) Field-induced charge transport at the surface of pentacene single crystals: A method to study charge dynamics of two-dimensional electron systems in organic crystals. *J Appl Phys* 94(9):5800–5804.
8. Butko VY, Chi X, Lang DV, Ramirez AP (2003) Field-effect transistor on pentacene single crystal. *Appl Phys Lett* 83(23):4773–4775.
9. Goldmann C, et al. (2004) Hole mobility in organic single crystals measured by a "flip-crystal" field-effect technique. *J Appl Phys* 96(4):2080–2086.
10. Jurchescu OD, Baas J, Palstra TTM (2004) Effect of impurities on the mobility of single crystal pentacene. *Appl Phys Lett* 84(16):3061–3063.
11. Abthagir PS, et al. (2005) Studies of tetracene- and pentacene-based organic thin-film transistors fabricated by the neutral cluster beam deposition method. *J Phys Chem B* 109(50):23918–23924.
12. Gundlach DJ, Nichols JA, Zhou L, Jackson TN (2002) Thin-film transistors based on well-ordered thermally evaporated naphthacene films. *Appl Phys Lett* 80(16): 2925–2927.
13. Dimitrakopoulos CD, Malenfant PRL (2002) Organic thin film transistors for large area electronics. *Adv Mater* 14(2):99.
14. Cicoira F, et al. (2005) Correlation between morphology and field-effect-transistor mobility in tetracene thin films. *Adv Funct Mater* 15(3):375–380.
15. Lin YY, Gundlach DJ, Nelson SF, Jackson TN (1997) Stacked pentacene layer organic thin-film transistors with improved characteristics. *IEEE Electr Device L* 18(12): 606–608.
16. Kelley TW, Muyres DV, Baude PF, Smith TP, Jones TD (2003) High performance organic thin film transistors. *Mater Res Soc Symp P* 771:169–179.
17. Jurchescu OD, Popinciuc M, van Wees BJ, Palstra TTM (2007) Interface-controlled, high-mobility organic transistors. *Adv Mater* 19(5):688.
18. Gruhn NE, et al. (2002) The vibrational reorganization energy in pentacene: Molecular influences on charge transport. *J Am Chem Soc* 124(27):7918–7919.
19. Odom SA, Parkin SR, Anthony JE (2003) Tetracene derivatives as potential red emitters for organic LEDs. *Org Lett* 5(23):4245–4248.
20. Wolak MA, Jang BB, Palilis LC, Kafafi ZH (2004) Functionalized pentacene derivatives for use as red emitters in organic light-emitting diodes. *J Phys Chem B* 108(18): 5492–5499.
21. Jang BB, Lee SH, Kafafi ZH (2006) Asymmetric pentacene derivatives for organic light-emitting diodes. *Chem Mater* 18(2):449–457.
22. Picciolo LC, Murata H, Kafafi ZH (2001) Organic light-emitting devices with saturated red emission using 6,13-diphenylpentacene. *Appl Phys Lett* 78(16):2378–2380.
23. Chu CW, Shao Y, Shrotriya V, Yang Y (2005) Efficient photovoltaic energy conversion in tetracene-C-60 based heterojunctions. *Appl Phys Lett* 86(24):243506.
24. Yoo S, Domercq B, Kippelen B (2004) Efficient thin-film organic solar cells based on pentacene/C-60 heterojunctions. *Appl Phys Lett* 85(22):5427–5429.
25. Rand BP, Genoe J, Heremans P, Poortmans J (2007) Solar cells utilizing small molecular weight organic semiconductors. *Prog Photovolt Res Appl* 15(8):659–676.
26. Shao Y, Sista S, Chu CW, Sievers D, Yang Y (2007) Enhancement of tetracene photovoltaic devices with heat treatment. *Appl Phys Lett* 90(10):103501.
27. Mayer AC, Lloyd MT, Herman DJ, Kasen TG, Malliaras GG (2004) Postfabrication annealing of pentacene-based photovoltaic cells. *Appl Phys Lett* 85(25):6272–6274.
28. Singh S, Jones WJ, Siebrand W, Stoichef BP, Schneide WG (1965) Laser Generation of Excitons and Fluorescence in Anthracene Crystals. *J Chem Phys* 42(1):330.
29. Smith MB, Michl J (2010) Singlet fission. *Chem Rev* 110(11):6891–6936.
30. Smith MB, Michl J (2013) Recent advances in singlet fission. *Annu Rev Phys Chem* 64: 361–386.
31. Chan WL, et al. (2013) The quantum coherent mechanism for singlet fission: experiment and theory. *Acc Chem Res* 46(6):1321–1329.
32. Zimmerman PM, Bell F, Casanova D, Head-Gordon M (2011) Mechanism for singlet fission in pentacene and tetracene: from single exciton to two triplets. *J Am Chem Soc* 133(49):19944–19952.
33. Zimmerman PM, Zhang Z, Musgrave CB (2010) Singlet fission in pentacene through multi-exciton quantum states. *Nat Chem* 2(8):648–652.
34. Hanna MC, Nozik AJ (2006) Solar conversion efficiency of photovoltaic and photoelectrolysis cells with carrier multiplication absorbers. *J Appl Phys* 100(7):074510.
35. Tayebjee MJY, McCamey DR, Schmidt TW (2015) Beyond Shockley-Queisser: Molecular Approaches to High-Efficiency Photovoltaics. *J Phys Chem Lett* 6(12):2367–2378.
36. Zade SS, Bendikov M (2010) Heptacene and beyond: The longest characterized acenes. *Angew Chem Int Ed Engl* 49(24):4012–4015.
37. Marschalk C (1939) Linear hexacenes. *Bull Soc Chim Fr* 6:1112–1121.
38. Clar E (1939) Vorschläge zur Nomenklatur kondensierter Ringsysteme (Aromatische Kohlenwasserstoffe, XXVI. Mitteil.). *Ber Dtsch Chem Ges* 72(12):2137–2139.
39. Mondal R, Adhikari RM, Shah BK, Neckers DC (2007) Revisiting the stability of hexacenes. *Org Lett* 9(13):2505–2508.
40. Mondal R, Shah BK, Neckers DC (2006) Photogeneration of heptacene in a polymer matrix. *J Am Chem Soc* 128(30):9612–9613.
41. Tönshoff C, Bettinger HF (2010) Photogeneration of octacene and nonacene. *Angew Chem Int Ed Engl* 49(24):4125–4128.
42. Chakraborty H, Shukla A (2013) Correlated theory of linear optical absorption of octacene and nonacene. *J Phys Conf Ser* 454:012069.
43. Chakraborty H, Shukla A (2013) Large scale configuration interaction calculations of linear optical absorption of decacene. *AIP Conf Proc* 1538(1):271–275.
44. Ishida T, Aihara J (2009) Aromaticity of neutral and doubly charged polyacenes. *Phys Chem Chem Phys* 11(33):7197–7201.
45. Poater J, Bofill JM, Alemany P, Solà M (2005) Local aromaticity of the lowest-lying singlet states of [N]acenes (N = 6-9). *J Phys Chem A* 109(47):10629–10632.
46. Qu Z, Zhang D, Liu C, Jiang Y (2009) Open-shell ground state of polyacenes: A valence bond study. *J Phys Chem A* 113(27):7909–7914.
47. Sony P, Shukla A (2007) Large-scale correlated calculations of linear optical absorption and low-lying excited states of polyacenes: Pariser-Parr-Pople Hamiltonian. *Phys Rev B* 75(15):155208.
48. Bendikov M, et al. (2004) Oligoacenes: Theoretical prediction of open-shell singlet diradical ground states. *J Am Chem Soc* 126(24):7416–7417.
49. Hachmann J, Dorando JJ, Avilés M, Chan GK (2007) The radical character of the acenes: A density matrix renormalization group study. *J Chem Phys* 127(13):134309.
50. Hajgató B, Szieberth D, Geerlings P, De Proft F, Deleuze MS (2009) A benchmark theoretical study of the electronic ground state and of the singlet-triplet split of benzene and linear acenes. *J Chem Phys* 131(22):224321.
51. Hajgató B, Huzak M, Deleuze MS (2011) Focal point analysis of the singlet-triplet energy gap of octacene and larger acenes. *J Phys Chem A* 115(33):9282–9293.
52. Chai JD (2014) Thermally-assisted-occupation density functional theory with generalized-gradient approximations. *J Chem Phys* 140(18):18A521.
53. Rivero P, Jiménez-Hoyos CA, Scuseria GE (2013) Entanglement and polyradical character of polycyclic aromatic hydrocarbons predicted by projected Hartree-Fock theory. *J Phys Chem B* 117(42):12750–12758.
54. Gidofalvi G, Mazziotti DA (2008) Active-space two-electron reduced-density-matrix method: Complete active-space calculations without diagonalization of the N-electron Hamiltonian. *J Chem Phys* 129(13):134108.
55. Casanova D, Head-Gordon M (2009) Restricted active space spin-flip configuration interaction approach: Theory, implementation and examples. *Phys Chem Chem Phys* 11(42):9779–9790.

56. Ess DH, Johnson ER, Hu X, Yang W (2011) Singlet-triplet energy gaps for diradicals from fractional-spin density-functional theory. *J Phys Chem A* 115(1):76–83.
57. Peng D, et al. (2012) Variational fractional-spin density-functional theory for diradicals. *J Chem Phys* 137(11):114112.
58. Knippenberg S, Starcke JH, Wormit M, Dreuw A (2010) The low-lying excited states of neutral polyacenes and their radical cations: A quantum chemical study employing the algebraic diagrammatic construction scheme of second order. *Mol Phys* 108(19-20):2801–2813.
59. Goerigk L, Grimme S (2011) Double-hybrid density functionals provide a balanced description of excited (1)La and (1)Lb states in polycyclic aromatic hydrocarbons. *J Chem Theory Comput* 7(10):3272–3277.
60. Krykunov M, Grimme S, Ziegler T (2012) Accurate theoretical description of the (1)La and (1)Lb excited states in acenes using the all order constricted variational density functional theory method and the local density approximation. *J Chem Theory Comput* 8(11):4434–4440.
61. Kuritz N, Stein T, Baer R, Kronik L (2011) Charge-transfer-like $\pi \rightarrow \pi^*$ excitations in time-dependent density functional theory: A conundrum and its solution. *J Chem Theory Comput* 7(8):2408–2415.
62. Wong BM, Hsieh TH (2010) Optoelectronic and excitonic properties of oligoacenes: Substantial improvements from range-separated time-dependent density functional theory. *J Chem Theory Comput* 6(12):3704–3712.
63. Bettinger HF, Tönshoff C, Doerr M, Sanchez-Garcia E (2016) Electronically excited states of higher acenes up to nonacene: A density functional theory/multireference configuration interaction study. *J Chem Theory Comput* 12(1):305–312.
64. Richard RM, Herbert JM (2011) Time-dependent density-functional description of the (1)La state in polycyclic aromatic hydrocarbons: Charge-transfer character in disguise? *J Chem Theory Comput* 7(5):1296–1306.
65. Grimme S, Parac M (2003) Substantial errors from time-dependent density functional theory for the calculation of excited states of large pi systems. *Chemphyschem* 4(3): 292–295.
66. Kadantsev ES, Stott MJ, Rubio A (2006) Electronic structure and excitations in oligoacenes from ab initio calculations. *J Chem Phys* 124(13):134901.
67. Tozer DJ, Handy NC (2000) On the determination of excitation energies using density functional theory. *Phys Chem Chem Phys* 2(10):2117–2121.
68. Cave RJ, Zhang F, Maitra NT, Burke K (2004) A dressed TDDFT treatment of the 21Ag states of butadiene and hexatriene. *Chem Phys Lett* 389(1-3):39–42.
69. Ullrich C (2012) *Time-Dependent Density-Functional Theory: Concepts and Applications* (Oxford Univ Press, Oxford).
70. Maitra NT, Zhang F, Cave RJ, Burke K (2004) Double excitations within time-dependent density functional theory linear response. *J Chem Phys* 120(13):5932–5937.
71. Elliott P, Goldson S, Canahui C, Maitra NT (2011) Perspectives on double-excitations in TDDFT. *Chem Phys* 391(1):110–119.
72. Coto PB, Sharifzadeh S, Neaton JB, Thoss M (2015) Low-lying electronic excited states of pentacene oligomers: A comparative electronic structure study in the context of singlet fission. *J Chem Theory Comput* 11(1):147–156.
73. Marian CM, Gilka N (2008) Performance of the density functional theory/multireference configuration interaction method on electronic excitation of extended pi-systems. *J Chem Theory Comput* 4(9):1501–1515.
74. Zeng T, Hoffmann R, Ananth N (2014) The low-lying electronic states of pentacene and their roles in singlet fission. *J Am Chem Soc* 136(15):5755–5764.
75. van Aggelen H, Yang Y, Yang W (2013) Exchange-correlation energy from pairing matrix fluctuation and the particle-particle random-phase approximation. *Phys Rev A* 88(3):030501.
76. Peng D, Steinmann SN, van Aggelen H, Yang W (2013) Equivalence of particle-particle random phase approximation correlation energy and ladder-coupled-cluster doubles. *J Chem Phys* 139(10):104112.
77. Scuseria GE, Henderson TM, Bulik IW (2013) Particle-particle and quasiparticle random phase approximations: Connections to coupled cluster theory. *J Chem Phys* 139(10):104113.
78. Yang Y, van Aggelen H, Steinmann SN, Peng D, Yang W (2013) Benchmark tests and spin adaptation for the particle-particle random phase approximation. *J Chem Phys* 139(17):174110.
79. van Aggelen H, Yang Y, Yang W (2014) Exchange-correlation energy from pairing matrix fluctuation and the particle-particle random phase approximation. *J Chem Phys* 140(18):18A511.
80. Shenvi N, van Aggelen H, Yang Y, Yang W (2014) Tensor hypercontracted ppRPA: Reducing the cost of the particle-particle random phase approximation from O(r(6)) to O(r(4)). *J Chem Phys* 141(2):024119.
81. Yang Y, van Aggelen H, Yang W (2013) Double, Rydberg and charge transfer excitations from pairing matrix fluctuation and particle-particle random phase approximation. *J Chem Phys* 139(22):224105.
82. Peng D, van Aggelen H, Yang Y, Yang W (2014) Linear-response time-dependent density-functional theory with pairing fields. *J Chem Phys* 140(18):18A522.
83. Yang Y, Peng D, Lu J, Yang W (2014) Excitation energies from particle-particle random phase approximation: Davidson algorithm and benchmark studies. *J Chem Phys* 141(12):124104.
84. Zhang D, Peng D, Zhang P, Yang W (2015) Analytic gradients, geometry optimization and excited state potential energy surfaces from the particle-particle random phase approximation. *Phys Chem Chem Phys* 17(2):1025–1038.
85. Yang Y, Peng D, Davidson ER, Yang W (2015) Singlet-triplet energy gaps for diradicals from particle-particle random phase approximation. *J Phys Chem A* 119(20): 4923–4932.
86. Yang Y, Burke K, Yang W (2015) Accurate atomic quantum defects from particle–particle random phase approximation. *Mol Phys* 114(7-8):1189–1198.
87. Salem L, Rowland C (1972) Electronic properties of diradicals. *Angew Chem Int Ed Engl* 11(2):92.
88. Michl J (1977) Role of biradicaloid geometries in organic-photochemistry. *Photochem Photobiol* 25(1):141–154.
89. Jiang DE, Dai S (2008) Electronic ground state of higher acenes. *J Phys Chem A* 112(2):332–335.
90. Einholz R, Bettinger HF (2013) Heptacene: Increased persistence of a 4n+2 $\pi$-electron polycyclic aromatic hydrocarbon by oxidation to the 4n $\pi$-electron dication. *Angew Chem Int Ed Engl* 52(37):9818–9820.
91. Baerends EJ, Gritsenko OV, van Leeuwen R (1996) Effective one-electron potential in the Kohn–Sham molecular orbital theory. *Chemical Applications of Density-Functional Theory*, ACS Symposium Series (American Chemical Society, Anaheim, CA), Vol 629, pp 20-41.
92. Baerends EJ, Gritsenko OV (1997) A quantum chemical view of density functional theory. *J Phys Chem A* 101(30):5383–5403.
93. Stowasser R, Hoffmann R (1999) What do the Kohn–Sham orbitals and eigenvalues mean? *J Am Chem Soc* 121(14):3414–3420.
94. Casida ME (1996) Time-dependent density functional response theory of molecular systems: Theory, computational methods, and functionals. *Theoretical and Computational Chemistry*, ed Seminario JM (Elsevier, Amsterdam), Vol 4, pp 391–439.
95. dos Santos MC (2006) Electronic properties of acenes: Oligomer to polymer structure. *Phys Rev B* 74:045426.
96. Platt JR (1949) Classification of spectra of Cata-condensed hydrocarbons. *J Chem Phys* 17(5):484–495.
97. Peach MJ, Benfield P, Helgaker T, Tozer DJ (2008) Excitation energies in density functional theory: An evaluation and a diagnostic test. *J Chem Phys* 128(4):044118.
98. Guidez EB, Aikens CM (2013) Origin and TDDFT benchmarking of the plasmon resonance in acenes. *J Phys Chem C* 117(41):21466–21475.
99. Biermann D, Schmidt W (1980) Diels-Alder reactivity of polycyclic aromatic-hydrocarbons. 1. Acenes and benzologs. *J Am Chem Soc* 102(9):3163–3173.
100. Angliker H, Rommel E, Wirz J (1982) Electronic-spectra of hexacene in solution (ground-state, triplet-state, dication and dianion). *Chem Phys Lett* 87(2):208–212.
101. Mondal R, Tönshoff C, Khon D, Neckers DC, Bettinger HF (2009) Synthesis, stability, and photochemistry of pentacene, hexacene, and heptacene: A matrix isolation study. *J Am Chem Soc* 131(40):14281–14289.
102. Halasinski TM, Hudgins DM, Salama F, Allamandola LJ, Bally T (2000) Electronic absorption spectra of neutral pentacene (C22H14) and its positive and negative ions in Ne, Ar, and Kr matrices. *J Phys Chem A* 104(32):7484–7491.
103. Nijegorodov N, Ramachandran V, Winkoun DP (1997) The dependence of the absorption and fluorescence parameters, the intersystem crossing and internal conversion rate constants on the number of rings in polyacene molecules. *Spectrochim Acta A* 53(11):1813–1824.
104. Heinecke E, Hartmann D, Müller R, Hese A (1998) Laser spectroscopy of free pentacene molecules (I): The rotational structure of the vibrationless $S_1 \leftarrow S_0$ transition. *J Chem Phys* 109(3):906.
105. Cohen AJ, Mori-Sánchez P, Yang W (2008) Insights into current limitations of density functional theory. *Science* 321(5890):792–794.
106. Gritsenko OV, van Gisbergen SJA, Gorling A, Baerends EJ (2000) Excitation energies of dissociating H-2: A problematic case for the adiabatic approximation of time-dependent density functional theory. *J Chem Phys* 113(19):8478–8489.
107. Cohen AJ, Mori-Sánchez P, Yang W (2012) Challenges for density functional theory. *Chem Rev* 112(1):289–320.
108. Starcke JH, Wormit M, Schirmer J, Dreuw A (2006) How much double excitation character do the lowest excited states of linear polyenes have? *Chem Phys* 329(1-3): 39–49.
109. Mikhailov IA, Tafur S, Masunov AE (2008) Double excitations and state-to-state transition dipoles in pi-pi* excited singlet states of linear polyenes: Time-dependent density-functional theory versus multiconfigurational methods. *Phys Rev A* 77(1).
110. Pati YA, Ramasesha S (2014) Exact solution of the PPP model for correlated electronic states of tetracene and substituted tetracene. *J Phys Chem A* 118(23): 4048–4055.
111. Tomkiewi Y, Groff RP, Avakian P (1971) Spectroscopic approach to energetics of exciton fission and fusion in tetracene crystals. *J Chem Phys* 54(10):4504.
112. Frisch MJ, et al. (2009) *Gaussian 09* (Gaussian, Inc., Wallingford, CT).
113. QM4D, An in-house program for QM/MM simulations. Available at www.qm4d.info. Accessed July 31, 2016.
114. Lee C, Yang W, Parr RG (1988) Development of the Colle-Salvetti correlation-energy formula into a functional of the electron density. *Phys Rev B Condens Matter* 37(2): 785–789.
115. Becke AD (1993) Density-functional thermochemistry. III. The role of exact exchange. *J Chem Phys* 98(7):5648.
116. Dunning TH (1989) Gaussian basis sets for use in correlated molecular calculations. I. The atoms boron through neon and hydrogen. *J Chem Phys* 90(2):1007.
117. Birks JB (1970) *Photophysics of Aromatic Molecules* (Wiley-Interscience, London).
118. Schiedt J, Weinkauf R (1997) Photodetachment photoelectron spectroscopy of mass selected anions: Anthracene and the anthracene-H2O cluster. *Chem Phys Lett* 266(1-2):201–205.
119. Sabbatini N, Indelli MT, Gandolfi MT, Balzani V (1982) Quenching of singlet and triplet excited-states of aromatic-molecules by europium ions. *J Phys Chem-Us* 86(18):3585–3591.
120. Burgos J, Pope M, Swenberg CE, Alfano RR (1977) Heterofission in pentacene-doped tetracene single crystals. *Phys Status Solidi B* 83(1):249–256.